



OPEN Prediction of potential shear slip surface in locked rock mass of gently inclined counter Tilted rock slope under mining effects

Wenfu Meng^{1,2}, Zhangyin Dai^{1,2}✉, Qingli Luo^{1,2}, Hongwei Bai^{1,2}, Ting Xia^{1,2} & Yunqin Cao¹

In recent years, landslides triggered by underground mining have attracted much attention because of their high hazards and difficulties in prediction and forecasting. How to quickly and accurately determine the potential shear slip surface in locked rock mass of gently inclined counter tilted rock slope under mining action is crucial for the prevention and control of this type of landslide hazard. In this study, the deformation and damage characteristics of gently inclined counter tilted rock slope under mining action are investigated by numerical simulation, theoretical analysis and physical test, using the Meidong Slope as a prototype, the mathematical equations describing the damage of mining disturbance of slope are established, and a prediction model of the shear slip surface in locked rock mass of the slope is proposed. The results show that the prediction model can accurately determine the shear slip surface of the locked rock mass of the slope, the reinforcement of the locked rock mass is the key area for the prevention and control of this type of landslide disaster, and the results of the study can provide a reference for the prevention and control of the geologic disaster of the mountain instability induced by underground mining on gentle anti-dip rocky slopes.

Keywords Underground mining, Gentle anti-dip Rocky slope, Locked rock mass, Numerical simulation, Predictive modeling, Physical test

Gentle anti-dip rocky slopes are widely distributed in the mountainous regions of Southwest China and commonly exhibit deformation issues under the influence of mining activities. Research indicates that such landslides typically exhibit the characteristic feature of localized locked segments¹, with their stability governed by the dual mechanisms of the potential sliding surface and the rock mass mechanics of the locked segment. Based on this characteristic, previous studies have defined such slopes as locked-segment landslides². From an engineering geological perspective, the locked segment refers to the portion that plays a critical controlling role in slope stability^{3,4}. Essentially, it represents the unconnected part of the potential sliding surface^{5–8}. Due to their high shear strength and substantial geometric dimensions^{9–11}, locked segments can significantly enhance the overall load-bearing capacity of slopes, making them crucial in the stability analysis of rock slopes. Mining activities may induce progressive failure of the locked-segment rock mass, thereby triggering landslide disasters. Therefore, an in-depth study of the shear slip damage mechanism of locked segments in gentle anti-dip rocky slopes under mining disturbances will not only help reveal the instability mechanisms of such slopes but also provide a theoretical basis for optimizing slope protection design, reducing engineering costs, and improving stability, holding significant practical value for engineering applications.

Geological disasters induced by underground mining activities are increasingly common, particularly when mining operations are conducted beneath slopes, which can easily lead to slope deformation and instability¹². In recent years, related research has primarily been conducted through theoretical analysis, physical model testing, and numerical simulation. Malinowska et al.¹³ employed numerical models to analyze mining-induced strain fields and their effects on fracture formation; Fathi et al.¹⁴ took the instability of a high-steep slope induced by coal mining in Australia as an example, proposing that toe damage can lead to a composite sliding-toppling failure at the slope's leading edge; Regassa et al.¹⁵ investigated the relationship between mining depth and roof collapse; Zhao et al.¹⁶ revealed the formation mechanism of the Majialing landslide using PFC numerical simulation; Yu et al.¹⁷ employed the particle flow method to analyze the deformation characteristics of the Faer coal mine slope; Sun et al.¹⁸ obtained two failure modes—bending fracture of roadway strata and interlayer

¹Mining College, Guizhou University, Guiyang 550025, Guizhou, China. ²Complex Geological Mining Safety Technology Engineering Center, Guizhou University, Guiyang 550025, China. ✉email: zydai1@gzu.edu.cn

slip—through 3DEC modeling; Tang et al.¹⁹ proposed a landslide deformation mechanism controlled by “key blocks”; Tian et al.²⁰ demonstrated the “V”-shaped overburden failure pattern caused by stress release through physical simulation; Dai et al.^{21,22} used UDEC to study the dynamic evolution of slope deformation damage; Zhao et al.²³ found that the gentle anti-dip rocky slope at Majialing, Guizhou, formed a continuous sliding surface when the mining-damaged locked segment was sheared under water pressure. Liu et al.²⁴ simulated external excitations such as rainfall and earthquakes using a self-designed dynamic loading system to explore the progressive failure mechanism of “retaining wall-type” locked-segment landslides.

Although existing studies have revealed the influence mechanisms of mining on the deformation of gently inclined counter tilted rock slope through case analyses, theoretical models, and numerical simulations—confirming that the shearing of locked segments to form continuous sliding surfaces is a key factor triggering landslides—systematic research on the formation mechanism of potential shear slip surface in locked-segment rock masses of gentle anti-dip rocky slopes under mining disturbances remains lacking. Moreover, an effective method for quantitatively determining the spatial distribution characteristics of damage surfaces has yet to be established. Therefore, constructing a quantitative prediction model for shear slip surface in locked-segment rock masses under mining disturbances will not only provide a theoretical basis for precise early warning of landslide disasters but also offer scientific guidance for optimizing the design of engineering prevention and control measures, holding significant theoretical and practical importance.

Numerical simulation study

Basic geological condition

The Meidong Slope deformation is located in Duyun City, Guizhou Province, China, with the geographic coordinates of $107^{\circ}17'30''\sim 107^{\circ}18'28''\text{E}$ and $26^{\circ}10'35''\sim 26^{\circ}11'29''\text{N}$, see Fig. 1A and B. The recoverable coal seams in the study area are mainly located in the upper and middle parts of the Xiangbai Formation, which is composed of quartz sandstone and carbonaceous shale interbedded rocks, and is a typical gentle anti-dip rocky slope, see Fig. 1C. The geotectonic position of the well field is located in the east-south part of the north-south tectonic deformation zone of Guiding and Qiannan Plateau, a sub-tectonic unit of the Yangzi quasi-plateau, and the north-west flank of the southern section of the Huangshi Dorsal Plateau in the region, whose tectonic trajectory is characterized by the near-north-south oriented groove folds.

The study area has a long history of coal mining, dating back to the late 1990 s. The stratigraphy in the study area tends to the north-west, with a dip angle of $5\text{--}12^{\circ}$, from south-east to north-west, and the outcrops are, from old to new, the Upper Devonian Wangchengpo Formation (D_3w), the Devonian Zhewang Formation (D_3z), the Lower Carboniferous Tangbaigou Formation (C_1t), and the Carboniferous Xiangbai Formation (C_1x), and the coal-bearing stratigraphy is the Lower Carboniferous Xiangbai Formation, as shown in Fig. 2. There are only two mineable coal seams, A9 and A7, within the study area. The A9 seam is 1.71 ~ 1.95 m thick, with an average of 1.83 m, and the A7 seam is 1.61 ~ 1.81 m thick, with an average of 1.70 m. The lower part of the A9 seam is 15 ~ 25 m away from the A7 seam, and the average inclination angle of the coal seam is 7° .

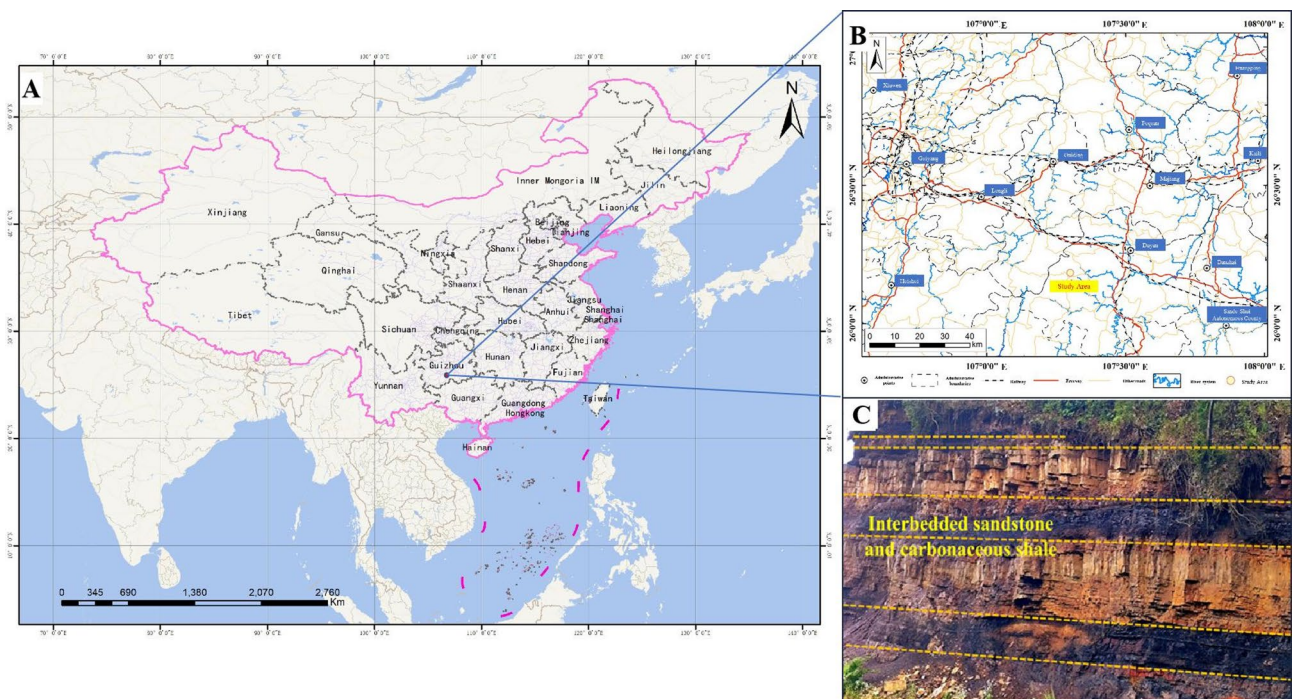


Fig. 1. (A) Location of Duyun City, Guizhou Province, China; (B) Location of deformation on Meidong Slope; “Figure A and B created with ArcGIS 10.8 (<https://www.esri.com>)” (C) Soft rock-hard rock interbedded structure.

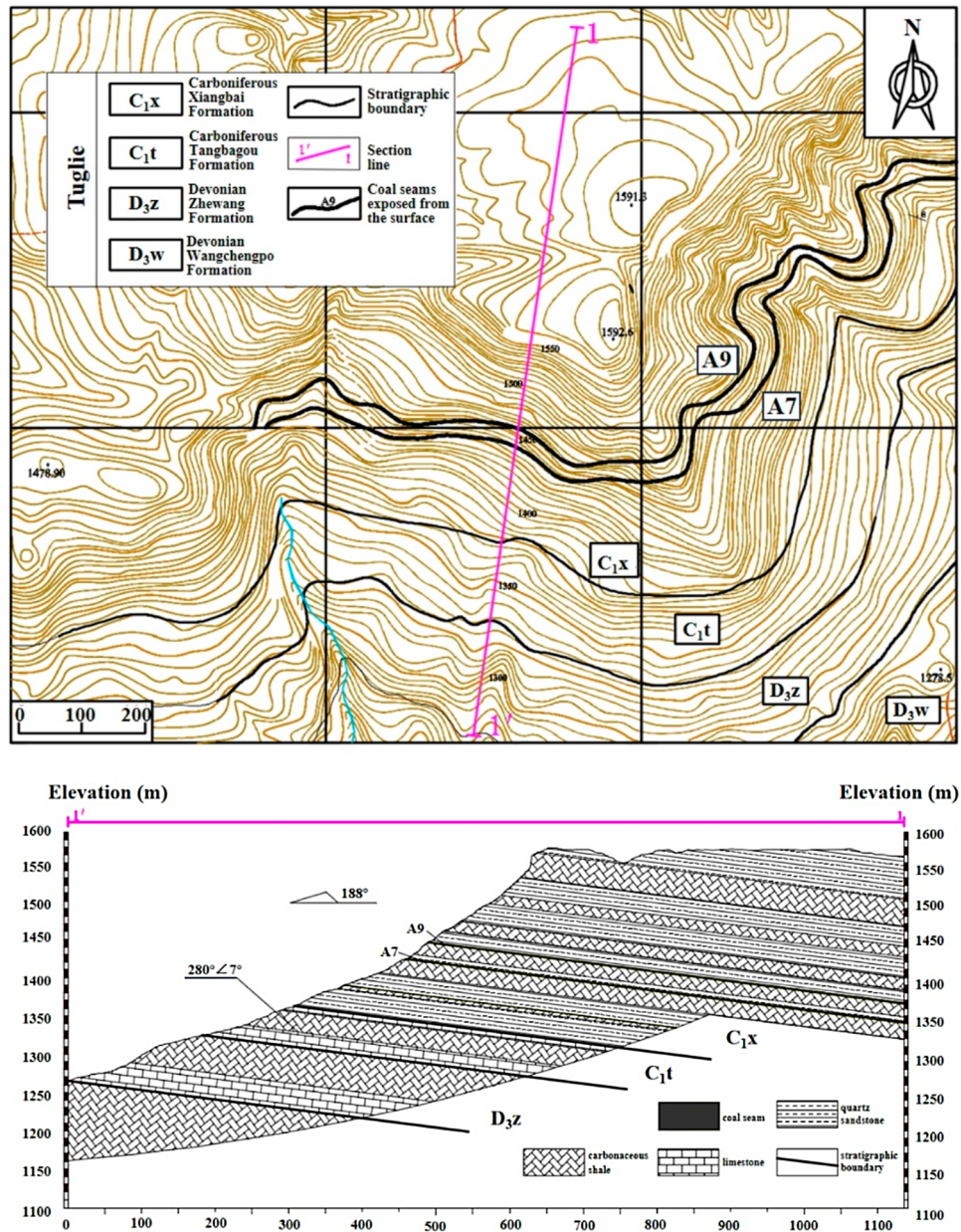


Fig. 2. Plan and section of engineering geology of Meidong Slope.

Numerical modeling

Based on the engineering geological section of the Meidong Slope in Fig. 2, because the rock layer below the A7 coal seam has less influence on the simulation, it is simplified to quartz sandstone, so as to establish the numerical model of the slope mass UDEC (Universal Distinct Element Code). And six displacement monitoring lines CX1, CX2, CX3, CX4, CX5 and CX6 are established, which are located at the soft rock-hard rock interbedding, as shown in Fig. 3.

The numerical slope model sets the rock joint orientation at 280°∠7° with orthogonal secondary joints. Both the coal and rock mass adopt the built-in Mohr-Coulomb constitutive model in UDEC software, while the joint surfaces utilize the Mohr-Coulomb slip model. The physico-mechanical parameters of coal-rock masses and joint parameters adopted in this study were all derived from laboratory investigations by Wang et al.²⁵⁻²⁷ with complete parameter specifications listed in Tables 1 and 2. The model constraints are zero horizontal displacement at the left and right boundaries of the slope, zero vertical displacement at the lower boundary, and a free boundary at the upper boundary.

Numerical calculations simulate the mining of coal seams A7 and A9 in the study area, and the design of the coal seams mining conditions is shown in Fig. 4, in the order of A9-01→A9-02→A7-01→A7-02. According to this design, the corresponding coal seams are mined sequentially to simulate repeated mining, and the iterative calculation of rock stress balance is carried out at the end of each mining task, and the next mining task is carried

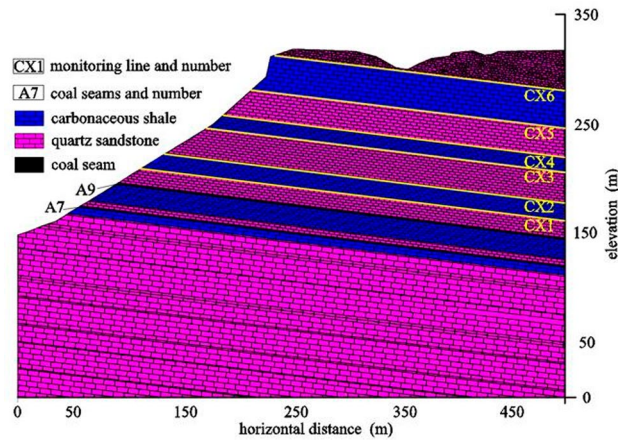


Fig. 3. Numerical model of Meidong Slope.

rock	density/(kg/m ³)	bulk modulus/GPa	tensile strength/MPa	internal friction angle/(°)	cohesion/MPa	Poisson's ratio
quartz sandstone	2500	15	0.91	42	28	0.19
carbonaceous shale	2200	5	0.52	37	15	0.25
coal	1700	0.5	0.31	36	0.43	0.31

Table 1. Parameters of the rock mass in the numerical simulation.

Structure plane	normal stiffness/GPa	shear stiffness/GPa	cohesion/MPa	internal friction angle/(°)
Rock layer	112	2.1	0.1	25

Table 2. Parameters of the joints in the numerical simulation.

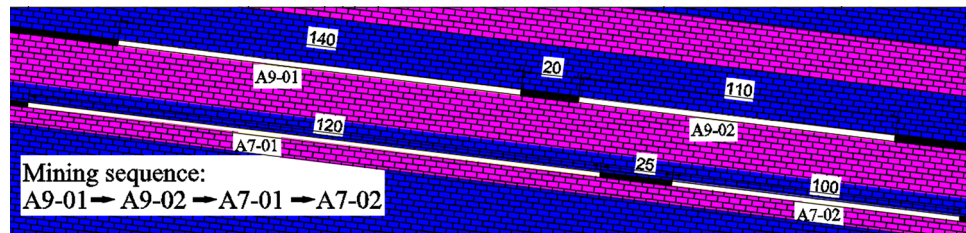


Fig. 4. Sequence of coal seam mining.

out at the end of the calculation. The length of each mining task: 140 m for A9-01 working face, 110 m for A9-02 working face, 200 m for A7-01 working face, 100 m for A7-02 working face, and the lengths of coal pillars left in A9 and A7 coal seams are 20 m and 25 m respectively.

Numerical simulation result analysis

Figure 5 shows a map of mining cracks at the end of mining, in which only cracks with a width greater than or equal to 0.01 m after mining of the coal seam are recorded, and the areas of mining cracks are shown in red. Figure 6 shows the vector map of slope displacement after the model repeats the end of mining in mining sequence, where the arrow points to the direction of displacement and the color represents the size of displacement. The rock above the coal pillar is better preserved due to the influence of the protective coal pillar, resulting in the mining fissure being clearly separated into two zones, contributing to the division of the slope into the front end of the slope and the back end of the slope (Fig. 5).

Repeated mining has caused the roof of the goaf to collapse and deform, and the overlying rock mass is severely fragmented, producing a large number of mining cracks (Fig. 5). The overall collapse of the overlying hard rock formations in the workings A9-01 and A7-01 goaf constitutes the front end of the slope, which is constrained by the gentle anti-dip strata and undergoes shear misalignment on the side close to the face of the slope, constituting a potential slip surface. There are fewer cracks in the collapse zone directly above the goaf,

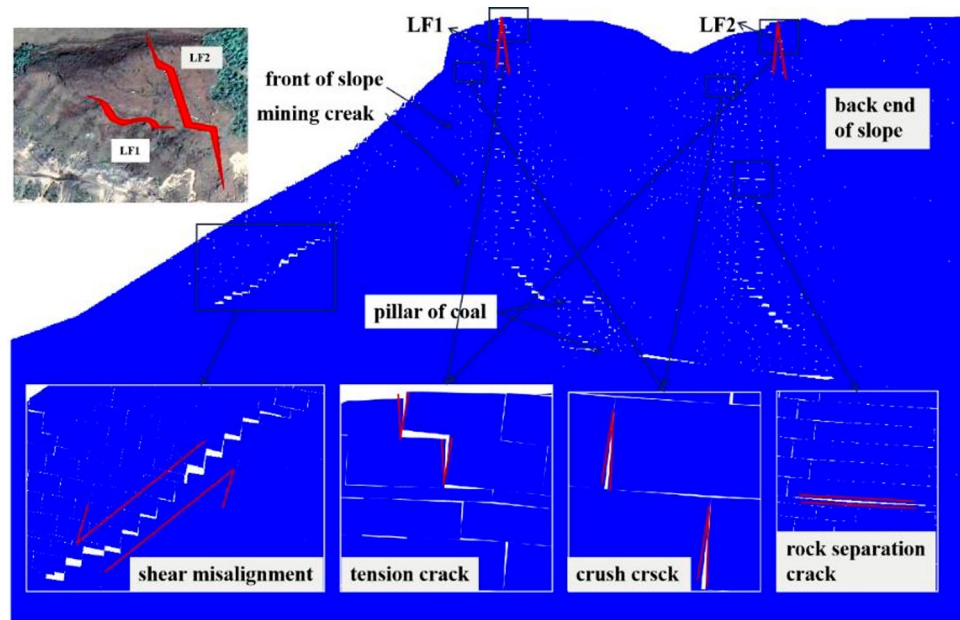


Fig. 5. Slope mining crack map.

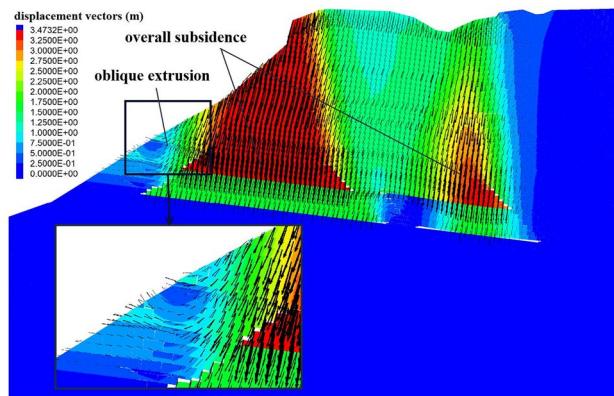


Fig. 6. Vector plot of slope displacement.

and this part of the cracks is closed by the extrusion of the rock body above, which can effectively block the expansion of the cracks. The cracks are centrally distributed on both sides of the goaf and spread upward, and then expand and develop around the collapsed rock mass to the central part to form the mining crack zone, and finally extend to the slope surface and the slope shoulder. The upper rock mass breaks down and sinks, and squeezes the lower rock mass to form the extrusion crack in the position of the slope shoulder, and the front end of the slope body produces the tendency of pouring downward to the slope surface, and forms the tensile crack LF1 in the position of the rear boundary.

The mining task A9-02 and A7-02 the upper rock mass of the goaf constitute the back end of the slope body. The cracks are uniformly distributed above the goaf and extend upward to the top of the slope, so that the rock mass at the top of the slope body is broken, the back end of the slope body is extruded and sunk above the front boundary to form an extrusion crack, and the back end of the slope body is tilted forward to form a tensile crack at the rear boundary. The cracks at the top of the slope develop through each other to form tensile cracks LF1 and LF2, and cracks LF1 and LF2 are generally consistent with field conditions.

Repeated mining resulted in the overall subsidence of the overlying rock mass in the goaf (Fig. 6), and the mining-induced settlement was transferred upward with gradually decreasing displacement. In mining task A9-01 and A7-01, the intact rock mass near the goaf near the slope formed a lock to the broken rock mass above, and at the same time, was also subjected to the oblique extrusion of the rock mass above, “elliptical arc” shaped displacement towards the slope, and accompanied by extrusion tendency, extrusion and uplift. Under the influence of the gentle anti-dip geology, the rock fragmentation above the back of the goaf has increased, and the zone of maximum displacement vector has generally moved back. The front end of the slope produces a tendency to dip towards the slope face, squeezing the lower part of the front boundary at the front end of the

slope and intensifying the fragmentation of the rock mass there, with an anomalous increase in the area of the maximum displacement vector, which extends upwards.

Figure 7 shows the vertical displacement curves of the numerical model soft-hard rock layers, and the arrangement of monitoring lines is shown in Fig. 3. After the end of coal seam mining, the vertical displacement curves of each monitoring line show “w” shape, the vertical displacement is between 0~−3.5 m. The rock mass above the mining task has the largest subsidence, and the rock mass above the coal pillar has the smallest subsidence. Based on the above analysis and the rock subsidence curve, the slope rock mass is roughly divided into five regions, I, II, III, IV and V, according to the vertical displacement of −1 m as the dividing line. Region II has the largest amount of subsidence, followed by region IV, while regions I, III, and V are relatively stable, and the amount of subsidence at the front end of region I is positive, extrusion and uplift deformation occurs.

Gentle anti-dip rocky slope mining deformation damage, cracks in the slope mass above the through the development of the formation of a potential slip surface, and to prevent the occurrence of landslide disaster mainly rely on the goaf near the slope near the integrity of the rock mass of the locking, locking the rock mass of the shear slip damage is the key to the occurrence of landslide disaster of this type of slopes. Spatially, the deformation damage is not uniformly distributed throughout the locked rock mass, For example, different rock layers at different locations are subjected to different extrusion pressures from the upper rock mass; The locking rock mass contains carbonaceous shale beds, quartz sandstone beds, and coal beds, and the extent of damage when the rock faces of different lithologies are subjected to extrusion shear varies. Therefore, determining the potential shear slip surface of locked rock masses can provide an important basis for preventing and controlling the occurrence of such landslides.

Predictive modeling of shear slip surface in locked rock mass

Building geometric model

According to the numerical simulation results, in order to determine the potential shear slip surface of the locked rock mass, this study constructs a geometric model of the anti-dip rocky slope after mining deformation and damage, and roughly divides the rock mass of the slope into five areas: locked area (I), proximity-disturbed and fragmented area (II), coal pillar protection area (III), disturbed and fragmented area (IV) and undisturbed area (V), Fissure LF1 and Fissure LF2 are located above the rear boundaries of Areas II and IV, respectively, see Fig. 8.

The I region is mainly subjected to the oblique slope ward compression of the crushed rock mass within the slope, and this section impedes the sliding of the crushed rock mass towards the slope. II and IV region is affected by coal seam mining, the rock mass is broken, the vertical displacement is greater than 1 m, and because of the influence of gentle anti-dip geology, the rock mass above the back of the goaf is broken intensified, the maximum vertical displacement range is generally shifted back, and II region of the slope produces a tendency to pour to the slope surface, extrusion of the front end of the lower part of the rock mass, so that the rock mass in this place is broken intensified and the maximum vertical displacement there is paradoxical increase. In this area constitutes a potential slip surface, the for the rock mass in this region, with the slope fragmentation and stress rebalancing, the complete rock mass gradually becomes smaller, limit equilibrium analysis of the model is simplified to build a potential slip surface, only consider the upper part of the slip surface of the more complete and effective rock mass. III region is located above the protected coal pillar, and V region is located at the back of the slope, where the rock mass is preserved more intact, with a vertical displacement of less than 1 m, and is less affected by the mining of coal seams.

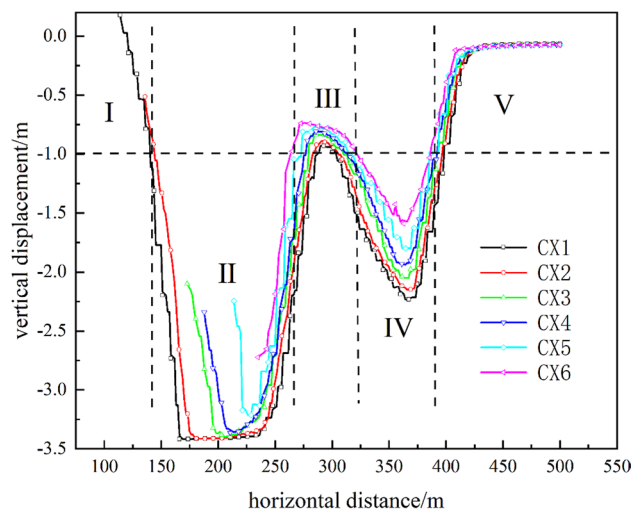


Fig. 7. Vertical displacement curve of rock formation.

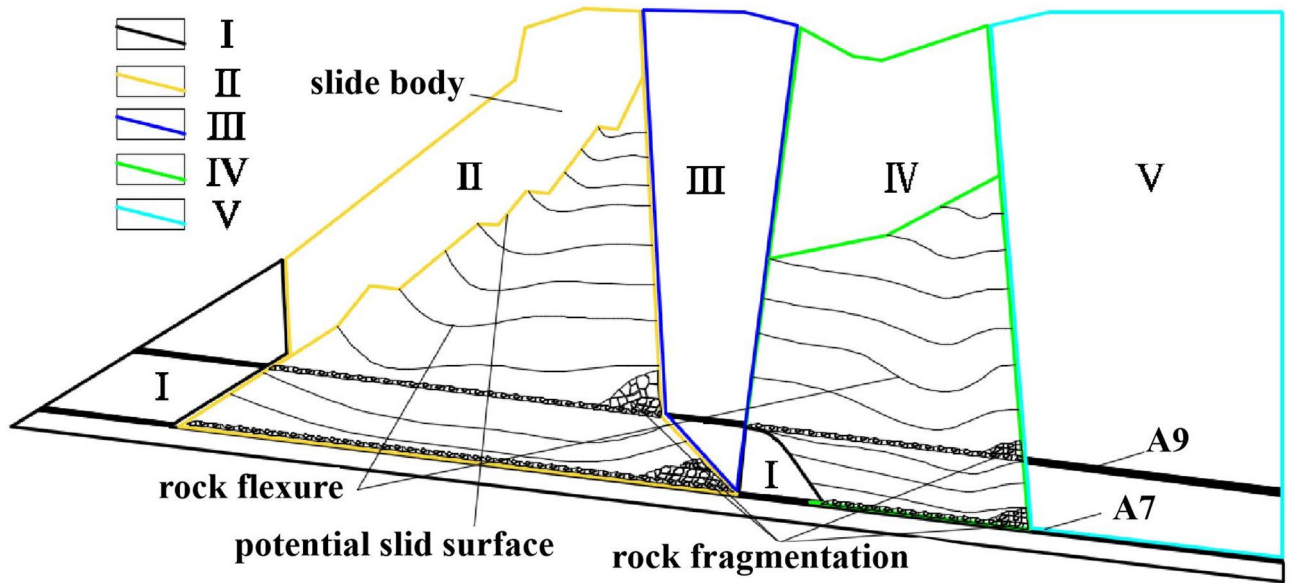


Fig. 8. Geometrical modeling of slope mining damage.

Predictive modeling of shear slip surface in locked rock masses

In order to determine the potential shear slip surface of the locked rock mass, the stability of the slope was analyzed by limit equilibrium analysis based on the geometric model of the anti-dip rocky slope after mining deformation and damage, as shown in Fig. 9.

The force analysis of the rock mass in Fig. 9(a) is:

$$G_i = \frac{(L_{01} + L_{02})}{2} h_i r_i \tag{1}$$

$$N_i = G_i \sin \alpha \cos \alpha \tag{2}$$

where G_i is the mass of the effective rock mass in the upper part of area IV after the slope is stabilized by mining; N_i is the external force on the effective rock mass; L_{01} and L_{02} are the lower and upper base lengths of the effective rock mass; h_i is the height of the effective rock mass; r_i is the unit mass of the effective rock mass; α is the angle between the lower slope of the effective rock mass and the horizontal plane.

Force analysis of the rock mass in Fig. 9(b):

$$N_i = N_{i+1} \tag{3}$$

where N_i and N_{i+1} are a pair of mutually balanced forces acting on the Region III rock mass.

According to the Mohr-Coulomb strength theory, the force analysis of the rock mass in Fig. 9(c) can be obtained as:

$$G_1 = \left[\frac{L_1^2}{2} \tan \theta + \frac{H - h_0}{\sin \theta} h \right] r_1 \tag{4}$$

where G_1 is the mass of the Region II slide after slope mining stabilization; L_1 is the length of the upper edge of the triangular rock mass on the upper part of the slide; H is the height of the slip surface; h_0 is the height of the slip surface of Region I; h is the height of the trapezoidal rock mass in Region II; r_1 is the mass per unit of the slide in Region II; θ is the angle of the side slope.

$$F_1 = (G_1 \cos \theta - N_{i+1} \sin \theta) \tan \phi + C \left(\frac{H - h_0}{\sin \theta} \right) \tag{5}$$

where F_1 is the slip resistance of the Region II slide; ϕ and C are the strength parameters of the structural surface; N_{i+1} is the force of the Region III rock mass acting on the Region II slide.

$$F_3 = G_1 \sin \theta + N_{i+1} \cos \theta \tag{6}$$

$$N_{i+2} = F_3 - F_1 \tag{7}$$

where F_3 is the sliding force generated by the gravity of the Region II slide itself; N_{i+2} is the force exerted by the Region II slide on the Region I locked rock mass.

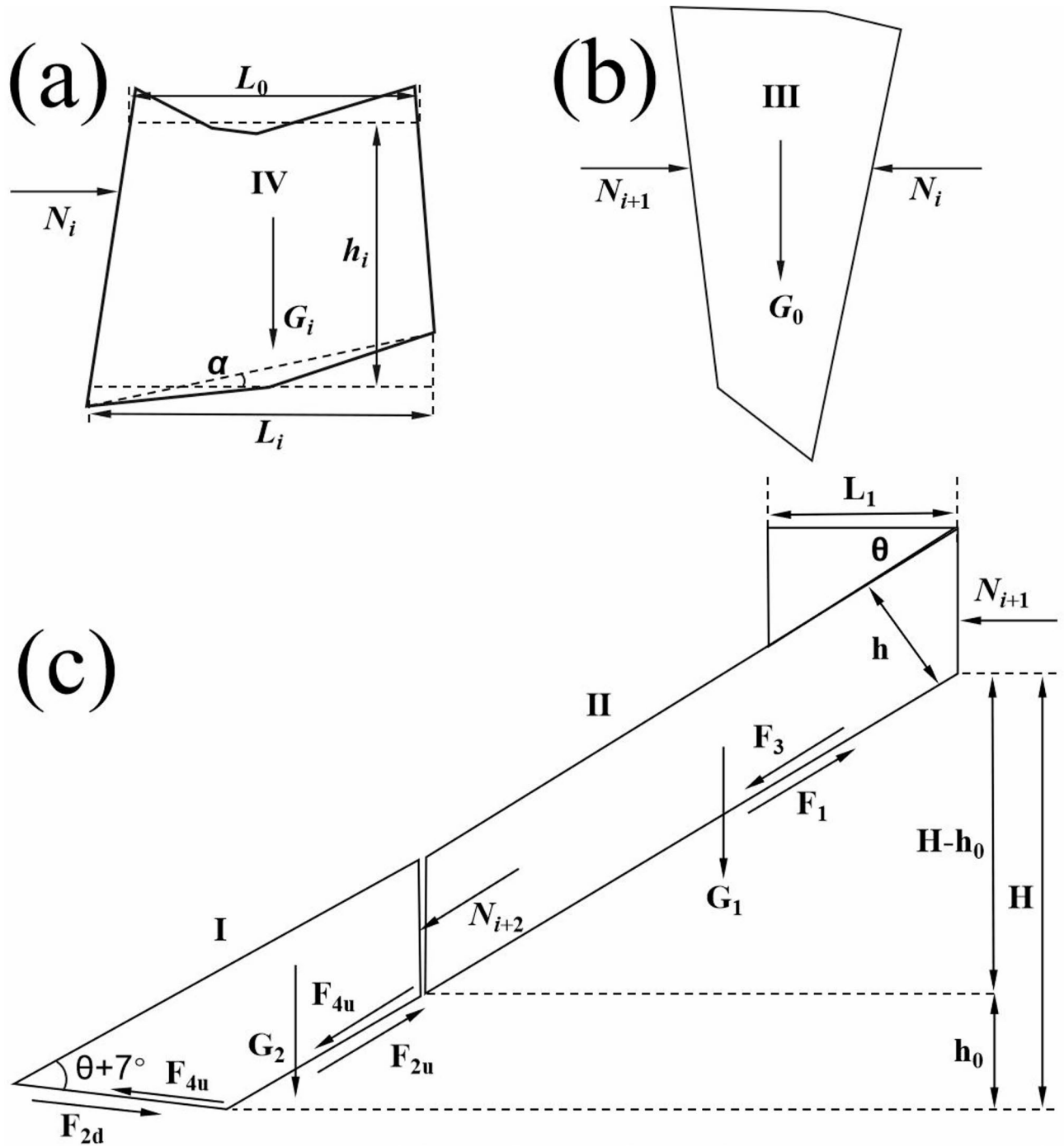


Fig. 9. Slope limit equilibrium analysis model; (a) Disturbed crushed zone IV rock mass; (b) Coal pillar protection zone III; (c) Locked zone II and proximity disturbed crushed zone II slip mass.

$$G_2 = \left[\frac{2h_0}{\sin\theta} + h \tan\theta + \frac{h}{\tan(\theta + 7^\circ)} \right] \frac{hr_2}{2} \tag{8}$$

where r_2 is the unit mass of the locked rock mass; G_2 is the mass of the locked rock mass in Area I after the slope mining stabilization; $\theta + 7^\circ$ is the angle between the slope surface and the structural surface.

$$F_{2u} = G_2 \cos\theta \tan\phi + C \frac{h_0}{\sin\theta} \tag{9}$$

$$F_{2d} = \left[N_{i+2} \sin(\theta + 7^\circ) + G_2 \cos^2\theta \right] \tan\phi + C \frac{h}{\sin(\theta + 7^\circ)} + G_2 \cos\theta \sin(\theta + 7^\circ) \tag{10}$$

Destroy the rock face	A9 coal rock	carbonaceous shale	quartz sandstone	A7 coal rock
h_0/m	7.75	26.19	27.32	29.36
H/m	132	147.32	152.38	154.38
$r_2/(kN \cdot m^{-3})$	23.48	22.92	23.17	22.93
F_s	1.1068	1.1576	1.1734	1.1777

Table 3. Calculation of damage surface prediction model.

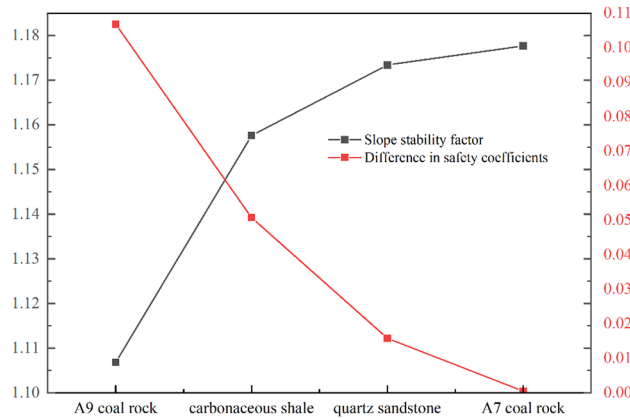


Fig. 10. Slope stabilization coefficients for the various formations of the locked rock mass.

where F_{2u} is the sliding resistance at the upper base of the locked rock; F_{2d} is the sliding resistance at the lower base of the locked rock.

$$F_{4u} = G_2 \sin \theta + N_{i+2} \tag{11}$$

$$F_{4d} = (G_2 \sin \theta + N_{i+2}) \cos (\theta + 7^\circ) \tag{12}$$

where F_{4u} and F_{4d} are the sliding forces on the locked rock mass.

Slope stability coefficient is the ratio of anti-slip force to sliding force along the assumed sliding surface, because the tilted tensile cracks at the trailing edge of the slide mass can not provide anti-slip force, the stability coefficient of anti-dip rocky slopes after mining deformation and damage F_s as:

$$F_s = \frac{F_k}{F_x} = \frac{F_1 + F_{2u} + F_{2d}}{F_3 + F_{4u} + F_{4d}} \tag{13}$$

where F_k is the total slip resistance of the slope after mining stabilization; F_x is the total sliding force on the slope.

The potential shear slip surface of the locked rock mass is determined by calculating and comparing the stability coefficient F_s after mining deformation damage of the anti-dip rocky slopes. Therefore, in order to simplify the stability calculations and determine the potential shear slip surface of the locked rock mass, the nonlinear variation process of the external force N_{i+1} in time and space is neglected in this paper. The increase of this external force will accelerate the shear slip damage of the locked rock mass, but it does not affect the determination of the potential shear slip surface, so it is assumed that the external force is 0.

$$F_s = \frac{[G_1 + G_2 - G_1 \sin(\theta + 7^\circ) \tan \phi] \cos \theta \tan \phi + C \left[\frac{H - (H - h_0) \sin(\theta + 7^\circ) \tan \phi}{\sin \theta} + \frac{h}{\sin(\theta + 7^\circ)} \right] + (G_1 \sin \theta \tan \phi + G_2 \cos \theta) \sin(\theta + 7^\circ)}{[2G_1 + G_2 + G_2 \cos(\theta + 7^\circ)] \sin \theta - (1 + \cos(\theta + 7^\circ)) \left[G_1 \cos \theta \tan \phi + C \left(\frac{H - h_0}{\sin \theta} \right) \right]} \tag{14}$$

In the formula, θ is 32° , L_1 is taken as 45.31 m, h is taken as 32 m, and r_1 is taken as 23.54 kN/m^3 , H , h_0 and r_2 are changed with the change of the calculation of the locking rock mass rock face. The slope stability coefficients of the locking rock mass at each level are calculated according to Eq. (14), and the calculation results are shown in Table 3.

When the stability coefficient is 1, the slope resistance is equal to the sliding force, at this time the slope is in the limit state of critical slip; when the ratio is less than 1, the slope is damaged; greater than 1, the slope is stable, and the larger the ratio the more stable the slope is; Define the difference of slope stability coefficient of each layer of locked rock mass is called stability difference, in which A9 coal seam is compared with the hypothetical damage surface, i.e., the difference of hypothetical damage surface with slope stability coefficient of 1. The slope stability coefficients and stability differences of each layer of locked rock mass are obtained as shown in Fig. 10.

Instrumentation	Specifications	Photograph
3D Full-field Deformation Measurement and Analysis System	Input voltage: 220 V 50 Hz AC Single/double camera lens: optional 8 mm, 16 mm, 25 mm, 35 mm Light source: 20 W, 180 and 200 W Beam: 500 mm and 1000 mm Control box: output frequency 10 Khz; power supply 120 W	
Earth Pressure Sensor	Measuring range: 100 kPa Overload capacity: 120% Connection mode: full bridge Accuracy error: ≤ 0.05 Electrical impedance: 350 Ω Bridge sensor: bridge voltage 2 V	
Wireless Static Strain Testing Systems	Bridge voltage: 2 V Measuring range: $\pm 15000 \mu\epsilon$ Strain gauge resistance: 50 ~ 20000 Ω Accuracy error: $\pm 0.2\%FS \pm 1 \mu\epsilon$ Power consumption: 11.1 V/0.3 A Battery capacity: 11.1 V/4.5 AH	

Table 4. Specification of measuring instruments for the physical model test.

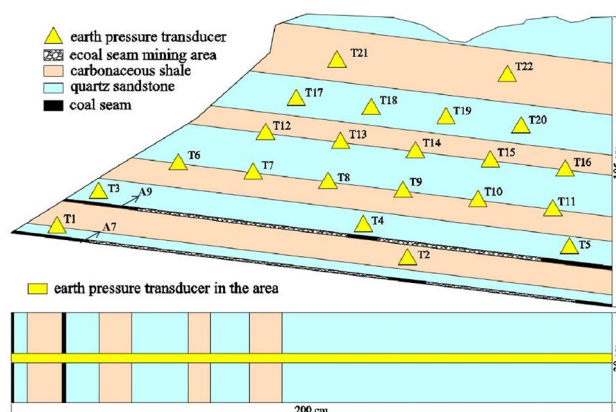


Fig. 11. Physical model design.

As can be seen from the data in Table 3 and the trends in Fig. 10, after the mining deformation damage of this anti-dip slope, the slope as a whole is still in a more stable state, and by comparing the slope stability coefficients, it is determined that the potential shear slip surface of the locking rock mass is the A9 coal seam. The mathematical model can provide a reference for predicting the shear slip damage level of locked rock mass after mining deformation damage of anti-dip rocky slopes to enhance landslide disaster prevention.

Physical test validation

Experimental design

The main parameters of the similarity simulation test include geometric size L , deformation modulus E , density, cohesion C , internal friction angle φ , and Poisson's ratio ν . According to the similarity theory and the similarity theorem, and taking into account the effective scale of the test platform, it is determined that the similarity constant of the test is selected to be $C = 200$, so that $CL = CE = C\gamma = CC = 200, C_\varphi = C\mu = 1$. The symbol C denotes the similarity ratio and the subscripts indicate the corresponding physical parameters. From the similarity constants combined with the engineering geological profile of the Meidong Slope (Fig. 2), the dimensions of the test model were determined as: length \times width \times height = 200 cm \times 30 cm \times 105 cm. The test uses soil pressure sensors (T1 ~ T22) to collect the model data, 3D Full-field Deformation Measurement and Analysis System to monitor the slope deformation data, the specific parameters of the testing instrument are shown in Table 4, and the arrangement of soil pressure sensors in the model is shown in Fig. 11.

Based on the previous study on the rock parameters of Meidong Slope²⁸, the similar materials consisted of barite powder, river sand, gypsum and cement, quartz sandstone composition (gypsum: cement: river sand: barite powder = 4: 2: 15: 15), carbonaceous shale composition (gypsum: cement: river sand: barite powder = 10: 1: 3: 2) and coal rock composition (gypsum: cement: river sand: barite powder = 1: 0: 10: 0), the mechanical parameters of similar materials are shown in Table 5.

According to the model design in Fig. 11, a physical test platform is built, as shown in Fig. 12. The model is stacked in layers, the similar materials are mixed well, and mica flakes are added to simulate the joint damage of the rock layer, after stacking one layer, a layer of mica flakes is sprinkled to simulate the structural surface of the

rock	density/(kg/m ³)	internal friction angle/(°)	cohesion/MPa
quartz sandstone	2460	43	141.6
carbonaceous shale	2140	37	78.7
coal	1680	36	3.4

Table 5. Mechanical parameters of similar materials.



Fig. 12. Test platform building.

rock layer, and the earth pressure transducer is buried in the corresponding position, and then the next layer of the model is stacked again. Mining action was simulated in the tests by manual excavation of similar material and adjustment of the bedrock support frame, and the coal seam was excavated in the same sequence as in Fig. 4.

Characterization and analysis of model deformation

The experiment uses the 3D Full-field Deformation Measurement and Analysis System to monitor slope deformation data. By processing the collected data, we obtain the displacement evolution maps and strain field evolution contour maps of the model under various design conditions. The displacement maps show the deformation of the model under coal mining conditions, while the strain maps represent the strain distribution under these conditions. Displacement maps focus on the absolute changes in position, whereas strain maps focus on the relative changes in internal material stress.

The evolution of the ensemble displacements generated by the model with each design condition mining is shown in Fig. 13. Figure 13a shows the initial shape of the model. When mining task A9-01 (Fig. 13b) and A9-02 (Fig. 13c), the overlying hard rock rock layer in the goaf collapses, the other rock mass combined displacement range is mainly distributed between 0.125 ~ 0.500 mm, and the locking rock mass does not have obvious change characteristics. When mining task A7-01 (Fig. 13d), under the influence of coal seam mining, the displacement of the slope mass increased greatly, mainly distributed between 0.250 ~ 1.625 mm, the displacement of the rock mass above the goaf of mining task A9-01 was larger, around 1.500 mm, and the displacement of the intact rock mass close to the slope surface was relatively small, below 1.000 mm, thus forming an obstacle to the sinking of the rock mass above the locking rock mass is initially formed by the shear effect. For the locking rock mass, it mainly contains carbonaceous shale rock layer, quartz sandstone rock layer and coal seam, in which the A9 coal seam is located in the location of the upper carbonaceous shale rock layer and the lower quartz sandstone rock layer compared with the larger displacement, more prone to shear slip damage. When mining task A7-02 (Fig. 13e), the slope displacement further increased, mainly distributed between 0.375 and 2.000 mm, and the displacement of the rock mass above the front end of the goaf in mining task A9-01 was the largest, reaching 2.000 mm, which formed a tiny shear misalignment with the intact rock mass close to the slope surface at the vicinity of the goaf and constituted a locking rock mass, hindering the dumping and sliding of the rock mass above in the direction of the slope surface. The maximum amount is 2,000 mm, and the maximum amount is 2,000 mm; The sinking of the upper rock mass also further squeezes the locking rock mass, and the locking rock

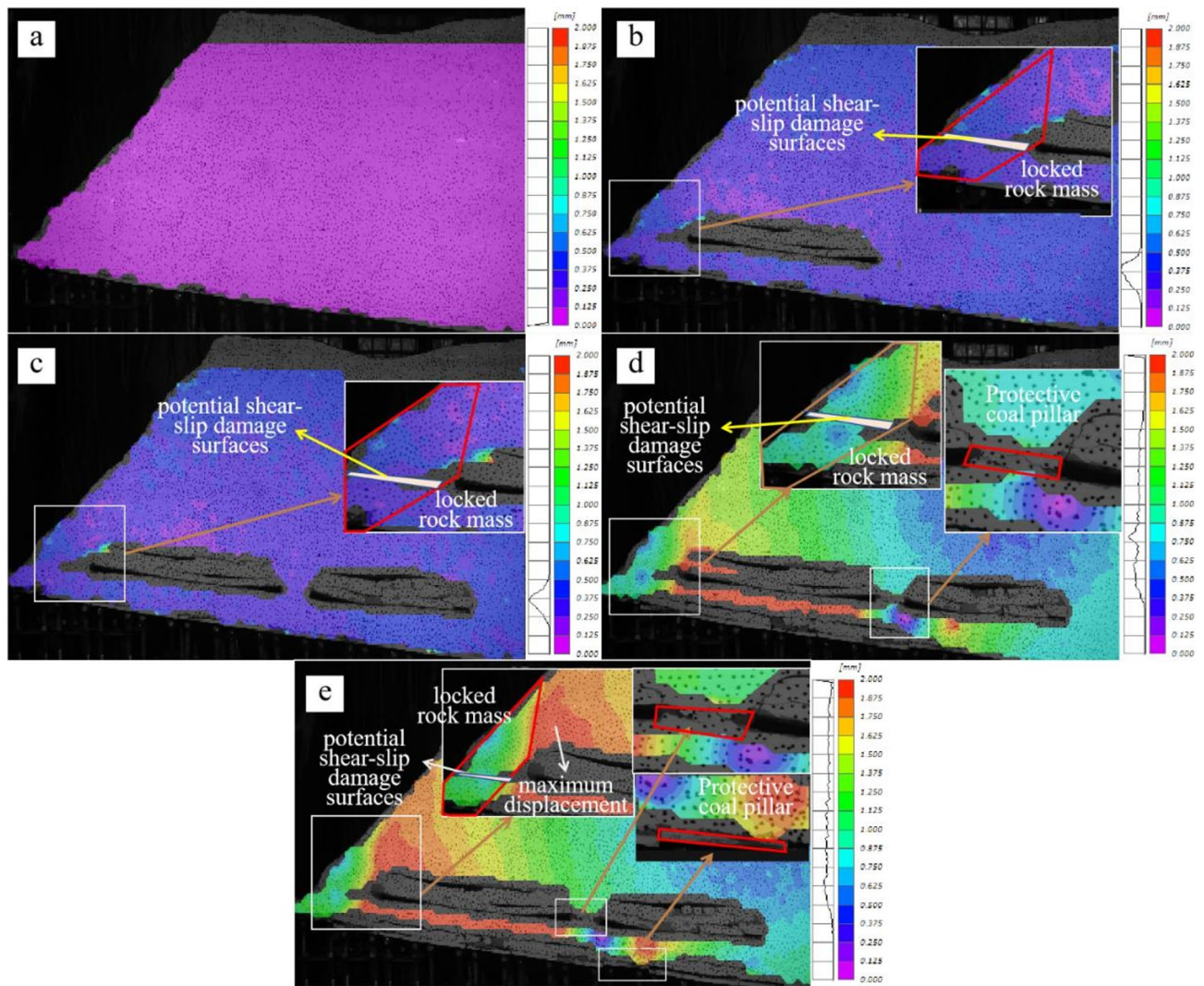


Fig. 13. Physical model combined displacement evolution cloud map.

mass is squeezed and sheared towards the slope face, and because the displacement of the A9 coal seam in the locking rock mass is significantly larger than that of the other rock seams, it proves that it is subjected to greater shear damage and is more likely to be subjected to shear slippage, and it is most probable that the potential shear slippage damage surface of the locking rock mass is the A9 coal seam.

A cloud diagram of the evolution of the strain field of the model with the mining task is shown in Fig. 14. Figure 14a shows the initial shape of the model. From Fig. 14b and c, the strain of the slope mass at mining task A9-01 and A9-02 is small, mainly concentrated in the rock mass above the goaf of mining task A9-01 and close to the slope, which is conducive to the formation of the locking rock mass. In mining task A7-01 (Fig. 14d) and A7-02 (Fig. 14e), the strain on the rock above the front end of the goaf in mining task A9-01 is larger, and the strain on the rock near the slope in the annex of the goaf is smaller, thus constituting a locking rock mass, which hinders the dumping and sliding of the rock above it in the direction of the slope. At this stage, the locked rock mass of the slope is controlled by shear stress, and at the same time, the slope continues to creep and slip, and the deformation increases, resulting in creep and slip damage to the locked rock mass and bulging. The strain of the rock stratum where the A9 coal seam is located in the locked rock mass is more than 70%, which is obviously larger than the other rock seams, proving that the disruption by deformation is more serious at this place, and the potential shear slip surface of the locked rock mass is the most likely for the A9 coal seam.

The earth pressure monitoring of the model as the workings are mined is shown in Fig. 15, and the layout of the earth pressure sensors is shown in Fig. 11. As can be seen from Fig. 16, the T1 sensor is located above the A7 coal seam in the locked rock body, and the normal stress varies from -5 to 10 kPa. After the end of mining of the working face A7-01, the stress redistribution of the side slopes leads to the decrease and then the increase of the positive stress above the A7 coal seam. This is due to the influence of the collapse of the overlying rock layer and the slow anticlinal strata in the mining hollow area, the positive stresses suffered from the A7 coal seam in the locked rock body can be released to reduce, again Because of the redistribution of stress in the rock mass leads to the concentration of stress at the front end, the positive stress increases sharply. The T3 sensor is located above

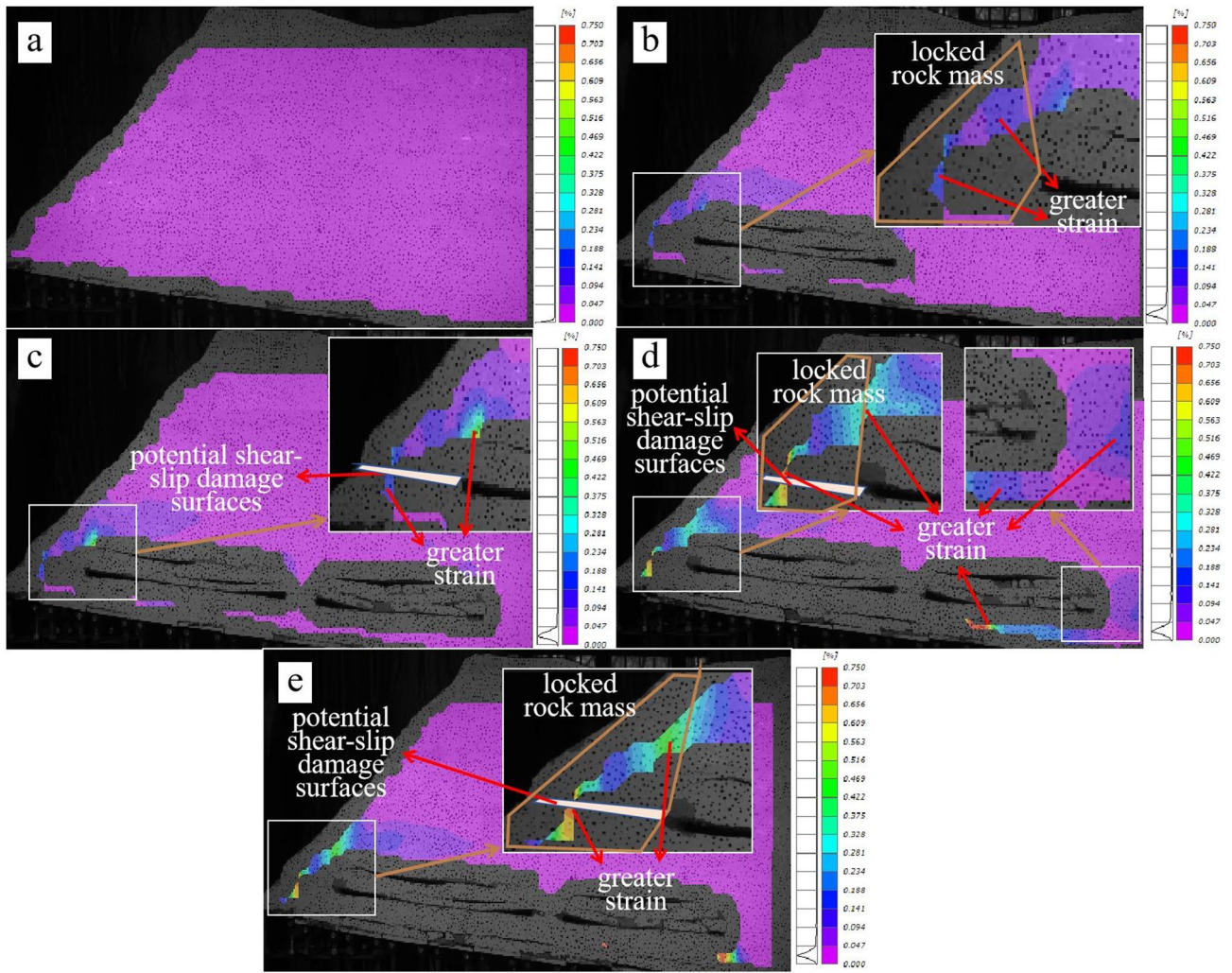


Fig. 14. Cloud diagram of the evolution of the strain field for physical models.

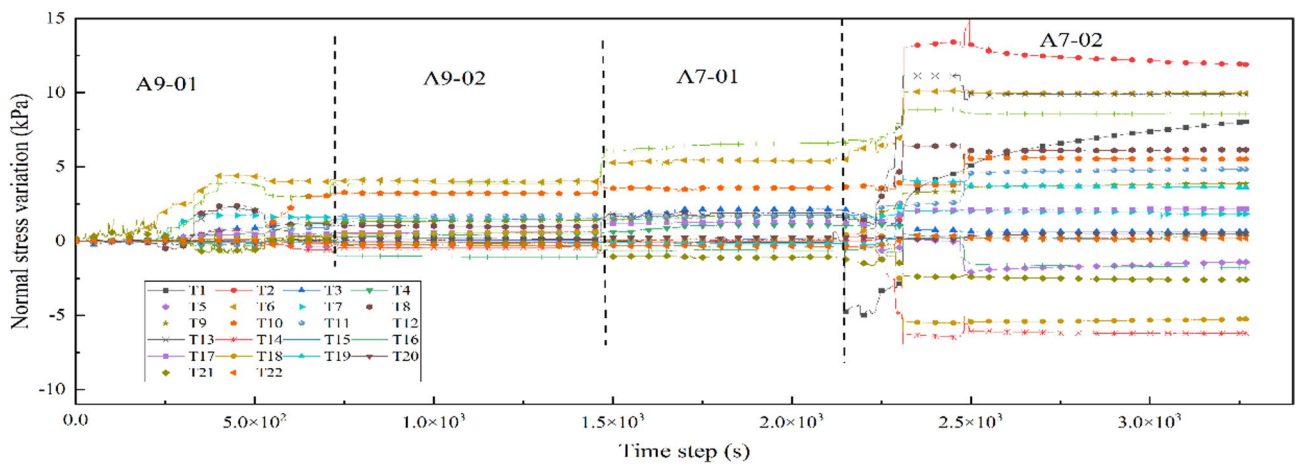


Fig. 15. Physical model normal stress monitoring.

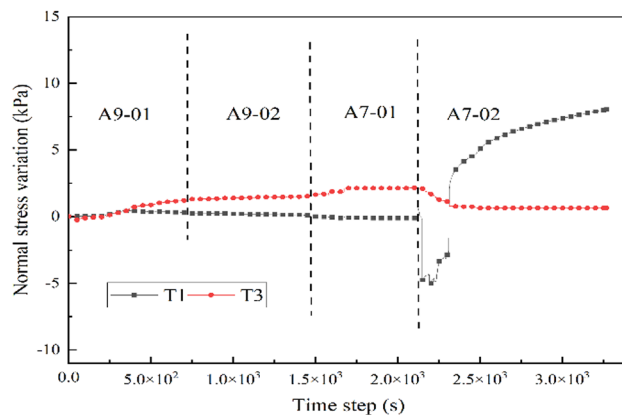


Fig. 16. T1 and T3 normal stress monitoring.

the A9 coal seam of the locked rock body, and the positive stress varies in the range of 0~2 kPa, which indicates that this location is first affected by the stress redistribution of the overlying rock layer in the mining area, and the positive stress increases, and then is supported by the collapsed rock body of the mining area after the end of the redistribution of the pressure of the slope rock body, and the positive stress decreases. Therefore, the positive stress on the A7 coal seam is greater than that on the A9 coal seam, which makes the slope slip resistance increase, and the potential shear slip surface of all locked rock bodies is most likely to be the A9 coal seam.

In summary, after the end of coal seam mining, the analysis of the combined displacement change, strain field evolution and normal stress change of the slope mass can determine the potential shear slip surface of the locking rock mass for the A9 coal seam, which is consistent with the results of the prediction model of the shear slip surface of the locking rock mass in this paper, and it proves that the prediction model can effectively predict the potential shear slip surface of the locking rock mass of the anti-dip slope under the mining action.

Limitation

Although the predictive modeling test for the potential shear slip surface of a rock body locked by a slow reverse slope under mining action has achieved relatively satisfactory results, there are still areas that need to be improved. First, the proposed model, due to the limitation of experimental conditions, only considers the influence of coal seam excavation on the model, but not the influence of external triggering factors, such as the time-varying process of rainfall and the creep behavior of the rock body. Secondly, although the prediction results of the potential shear-sliding damage surface of the rock body locked by the slow reverse slope were demonstrated by physical experiments, the experiments were carried out only once, and the reproducibility of the experiments needs to be fully considered. Finally, the feasibility of the model in the experiment was only verified in the laboratory, and its practical use needs to be further investigated to strengthen its practical relevance.

Conclusion

This study systematically investigates the prediction of potential shear slip surface in locked rock mass of gently inclined counter tilted rock slope under mining effects through an integrated approach combining numerical simulation, physical testing, and theoretical analysis. The main conclusions are as follows:

(1) The failure characteristics and formation mechanisms of locked rock masses in counter-tilted slopes under mining disturbance were investigated. The results demonstrate that the closer the mining position is to the slope surface, the more pronounced its impact on slope stability. Under gently counter-tilted stratigraphic conditions, the intact rock mass near the slope surface forms locked segments that create a restraining effect on the fractured slope above the goaf. The shear slip failure of these locked segments serves as a critical controlling factor triggering instability in such slopes.

(2) A predictive model for the potential shear slip failure surface of locked rock masses in counter-tilted slopes under mining action was established. Based on numerical simulation results, the slope rock mass was innovatively divided into five characteristic zones: locked area (I), proximity-disturbed and fragmented area (II), coal pillar protection area (III), disturbed and fragmented area (IV) and undisturbed area (V). The two-dimensional limit equilibrium method was then applied to analyze the stress state of the rock mass, constructing a predictive model capable of both quantifying the safety factor of mining-affected slopes and precisely locating the potential slip surface of locked rock masses. This model provides theoretical foundations and technical support for engineering reinforcement design.

(3) The predictive model was validated through numerical simulation and similarity simulation tests. The study reveals that post-mining slope deformation exhibits a composite “toppling-compression-shear” failure pattern. Comprehensive analysis of displacement fields, strain fields, and stress fields identified the A9 coal seam as the potential shear slip surface of the locked rock mass. These findings show excellent agreement with model predictions, confirming the accuracy and applicability of the proposed model.

Data availability

The datasets used and analysed during the current study available from the corresponding author on reasonable request.

Received: 22 January 2025; Accepted: 12 May 2025

Published online: 22 May 2025

References

- Havaej, M., Stead, D., Eberhardt, E. & Fisher, B. R. Characterization of bi-planar and ploughing failure mechanisms in footwall slopes using numerical modelling. *J Eng. Geol.* **178**, 109–120. <https://doi.org/10.1016/j.enggeo.2014.06.003> (2014).
- Qin, S. Q., Wang, Y. Y. & Ma, P. Exponential laws of critical displacement evolution for landslides and avalanches. *J Chin. J. Rock Mech. Eng.* **29** (5), 873–880 (2010).
- Huang, R. Q. Mechanisms of large-scale landslides in China. *J Bull. Eng. Geol. Environ.* **71** (1), 161–170. <https://doi.org/10.1007/s10064-011-0403-6e> (2011).
- Shao, C. J. et al. The role of active faults and sliding mechanism analysis of the 2017 Maoxian postseismic landslide in Sichuan, China. *J Bull. Eng. Geol. Environ.* **78** (8), 5635–5651. <https://doi.org/10.1007/s10064-019-01480-8> (2019).
- Elmo, D., Donati, D. & Stead, D. Challenges in the characterisation of intact rock bridges in rock slopes. *J Eng. Geol.* **245**, 81–96. <https://doi.org/10.1016/j.enggeo.2018.06.014> (2018).
- Tuckey, Z. & Stead, D. Improvements to field and remote sensing methods for mapping discontinuity persistence and intact rock bridges in rock slopes. *J Eng. Geol.* **208**, 136–153. <https://doi.org/10.1016/j.enggeo.2016.05.001> (2016).
- Zhang, K., Li, N., Liu, W. L. & Xie, J. B. Experimental study of the mechanical, energy conversion and frictional heating characteristics of locking sections. *J Eng. Fract. Mech.* **228**. <https://doi.org/10.1016/j.engfracmech.2020.106905> (2020).
- He, D. L., Yang, W. J., Cheng, Y. H. & Chen, B. C. Effect of anchor layouts on the safety factor and slip surface of slope. *J Geotech. Geol. Eng.* **37** (2), 1073–1078. <https://doi.org/10.1007/s10706-018-0655-z> (2019).
- Yang, B. C. et al. A physical self-similarity law describing the accelerated failure behavior of rocks. *J Chin. J. Geophys.* **60** (5), 1746–1760 (2017).
- Zhang, Q. H. et al. Study of the rock foundation stability of the Aizhai suspension Bridge over a deep Canyon area in China. *J Eng. Geol.* **198**, 65–77. <https://doi.org/10.1016/j.enggeo.2015.09.012> (2015).
- Zhao, X. Y., Hu, K., Liang, Y. & Yue, Z. Y. Experiment on sudden departure triggered by shearing vibration for locked segment of Wangjiayan landslide. *J Chin. J. Rock Mech. Eng.* **37** (1), 104–111. <https://doi.org/10.13722/j.cnki.jrme.2017.0438> (2018).
- Alejano, L. R., Ramirez-oyanguern, P. & Taboada, J. FDM predictive methodology for subsidence due to flat and inclined coal seam mining. *J Int. J. Rock Mech. Min. Sci.* **36** (4), 475–491. [https://doi.org/10.1016/S0148-9062\(99\)00022-4](https://doi.org/10.1016/S0148-9062(99)00022-4) (1999).
- Malinowska, A. A., Misa, R. & Tajdus, K. Geomechanical modeling of subsidence related strains causing Earth fissures. *J Acta Geodynamica Et Geomater.* **15** (2), 197–204. <https://doi.org/10.13168/agg.2018.0015> (2018).
- Fathi Salmi, E., Nazem, M. & Karakus, M. Numerical analysis of a large landslide induced by coal mining subsidence. *J Eng. Geol.* **217**, 141–152. <https://doi.org/10.1016/j.enggeo.2016.12.021> (2017).
- Regassa, B., Xu, N. X. & Mei, G. An equivalent discontinuous modeling method of jointed rock masses for DEM simulation of mining-induced rock movements. *J Int. J. Rock Mech. Min. Sci.* **108**, 1–14. <https://doi.org/10.1016/j.ijrmm.2018.04.053> (2018).
- Zhao, J. J., Xiao, J. G., Lee, M. L. & Ma, Y. T. Discrete element modeling of a mining-induced rock slide. *J Springerplus.* **5** (1), 1–19. <https://doi.org/10.1186/s40064-016-3305-z> (2016).
- Yu, J. L. et al. Deformation and failure of a high-steep slope induced by multi-layer coal mining. *J J. Mountain Sci.* **17** (12), 2942–2960. <https://doi.org/10.1007/s11629-019-5941-6> (2020).
- Sun, X. M. et al. Physical model test and numerical simulation on the failure mechanism of the roadway in layered soft rocks. *J Int. J. Min. Sci. Technol.* **31** (2), 291–302. <https://doi.org/10.1016/j.ijmst.2021.01.003> (2021).
- Tang, J. X., Dai, Z. Y., Wang, Y. L. & Zhang, L. Fracture failure of consequent bedding rock slopes after underground mining in mountainous area. *J Rock Mech. Rock Eng.* **52** (8), 2853–2870. <https://doi.org/10.1007/s00603-019-01876-8> (2019).
- Tian, M. L. et al. Physical model experiment of surrounding rock failure mechanism for the roadway under deviatoric pressure form mining disturbance. *J KSCE J. Civil Eng.* **24** (4), 1103–1115. <https://doi.org/10.1007/s12205-020-1540-x> (2020).
- Dai, Z. Y., Zheng, L. L., Wang, Y. L. & Zhou, H. Dynamic evolution law of deformation and failure of the bedding rock slope induced by the underground repeated mining activities. *J J. Saf. Environ.* **23** (06), 1807–1816. <https://doi.org/10.13637/j.issn.1009-6094.2021.2383> (2023).
- Dai, Z. Y., Liu, Q., Wang, Y. L. & Jiang, Z. B. Deformation and failure response of the bedding rock slope induced by the underground mining activities based on the distinctive element method. *J J. Saf. Environ.* **21** (03), 1089–1098. <https://doi.org/10.13637/j.issn.1009-6094.2020.0132> (2021).
- Zhao, J. J., Li, J. S., Ma, Y. T. & Yu, J. L. Experimental study on failure process of mining landslide induced by rainfall. *J J. China Coal Soc.* **45** (01), 760–769. <https://doi.org/10.13225/j.cnki.jccs.2019.0188> (2020).
- Liu, H. D. et al. Experimental study on the evolution mechanism of landslide with retaining wall locked segment. *J Geofluids.* **1**. <https://doi.org/10.1155/2022/7923448> (2022).
- Wang, Y. C. *Deformation Failure Mechanism and Stability Research of Massif above the Mined Out Area in Gently Inclined Coal Beds* (Chengdu University of Technology, 2013).
- Lai, Q. Y. et al. Deformation evolution of landslides induced by coal mining in mountainous areas: case study of the Madaling landslide, Guizhou, China. *J Landslides.* **20**, 2003–2016. <https://doi.org/10.1007/s10346-023-02069-9> (2023).
- Zhao, J. J. et al. Failure mechanism numerical simulation of mining landslide with gentle bedding coal strata. *J J. China Coal Soc.* **39** (03), 424–429. <https://doi.org/10.13225/j.cnki.jccs.2013.0365> (2014).
- Ma, Y. T. *Physical Simulation Study on Genetic Mechanism of Mining Landslide Under Rainfall ondition-take Madaling Landslide in Guizhou Province as an Example* (Chengdu University of Technology, 2017).

Acknowledgements

The research reported in this manuscript is funded by the National Natural Science Foundation of China (52264005).

Author contributions

W.M.: carried out experiments, collated and analyzed data, and wrote papers; Z.D.: supervised experiments, provided paper writing guidance, revised and polished manuscripts; T.X. and Q.L.: put forward ideas and theoretical analysis; H.B. and Y.C.: participated in the experiment and assisted in sorting out data and pictures. All authors agreed to the format and presentation of the final manuscript.

Declarations

Competing interests

The authors declare no competing interests.

Institutional review board statement

The study did not require ethical approval.

Additional information

Correspondence and requests for materials should be addressed to Z.D.

Reprints and permissions information is available at www.nature.com/reprints.

Publisher's note Springer Nature remains neutral with regard to jurisdictional claims in published maps and institutional affiliations.

Open Access This article is licensed under a Creative Commons Attribution-NonCommercial-NoDerivatives 4.0 International License, which permits any non-commercial use, sharing, distribution and reproduction in any medium or format, as long as you give appropriate credit to the original author(s) and the source, provide a link to the Creative Commons licence, and indicate if you modified the licensed material. You do not have permission under this licence to share adapted material derived from this article or parts of it. The images or other third party material in this article are included in the article's Creative Commons licence, unless indicated otherwise in a credit line to the material. If material is not included in the article's Creative Commons licence and your intended use is not permitted by statutory regulation or exceeds the permitted use, you will need to obtain permission directly from the copyright holder. To view a copy of this licence, visit <http://creativecommons.org/licenses/by-nc-nd/4.0/>.

© The Author(s) 2025